Journal Pre-proof

Nanobody-based retargeting of an oncolytic herpesvirus for eliminating CXCR4$^+$ GBM cells: a proof-of-principle

Judit Sanchez Gil, Maxime Dubois, Virginie Neirinckx, Arnaud Lombard, Natacha Coppieters, Paolo D'Arrigo, Damla Isci, Therese Aldenhoff, Benoit Brouwers, Cédric Lassence, Bernard Rogister, Marielle Lebrun, Catherine Sadzot-Delvaux

PII: S2372-7705(22)00078-X

DOI: https://doi.org/10.1016/j.omto.2022.06.002

Reference: OMTO 600

To appear in: *Molecular Therapy: Oncolytics*

Received Date: 5 May 2022

Accepted Date: 1 June 2022

Please cite this article as: Gil JS, Dubois M, Neirinckx V, Lombard A, Coppieters N, D'Arrigo P, Isci D, Aldenhoff T, Brouwers B, Lassence C, Rogister B, Lebrun M, Sadzot-Delvaux C, Nanobody-based retargeting of an oncolytic herpesvirus for eliminating CXCR4$^+$ GBM cells: a proof-of-principle, *Molecular Therapy: Oncolytics* (2022), doi: https://doi.org/10.1016/j.omto.2022.06.002.

CXCR4-retargeted oHSV

CXCR4 specific Nanobody

In vitro

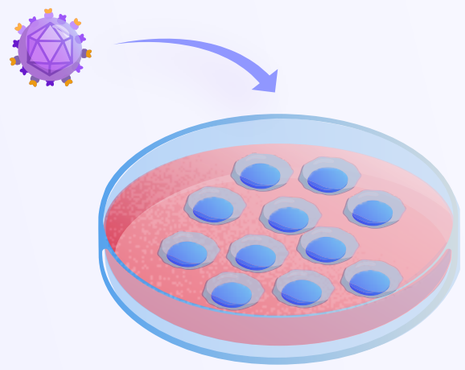

U87MG

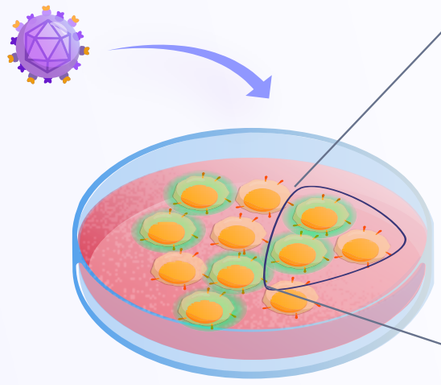

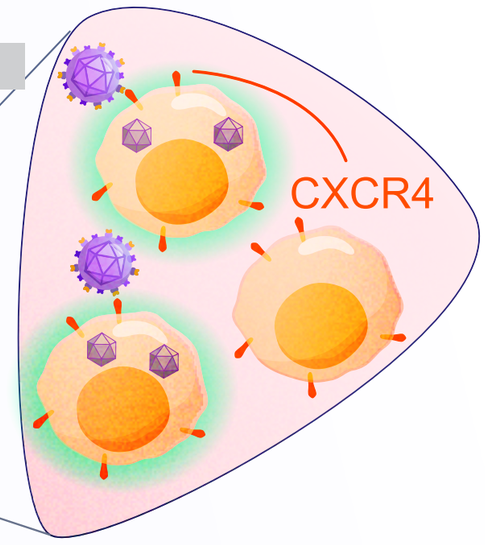

U87MG CXCR4

Ex vivo

Patient with glioblastoma

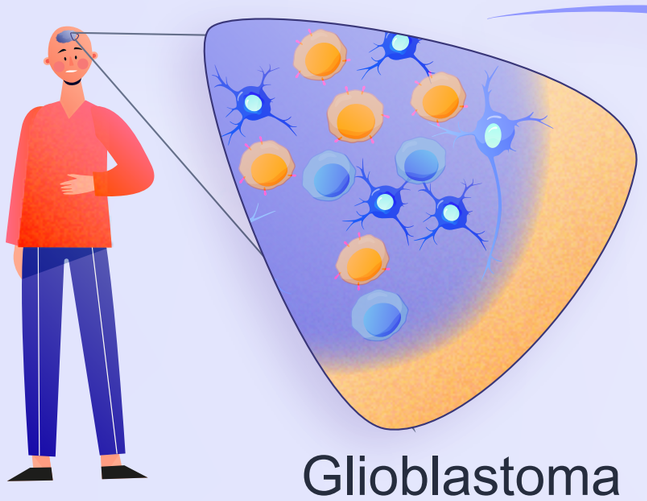

Glioblastoma

Enrichement in GSC

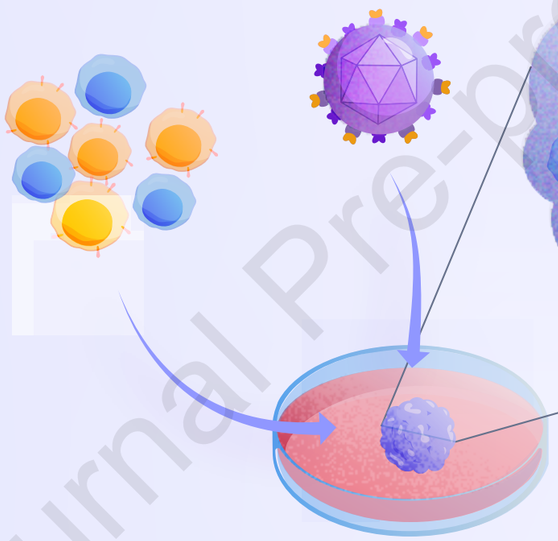

Tumorosphere

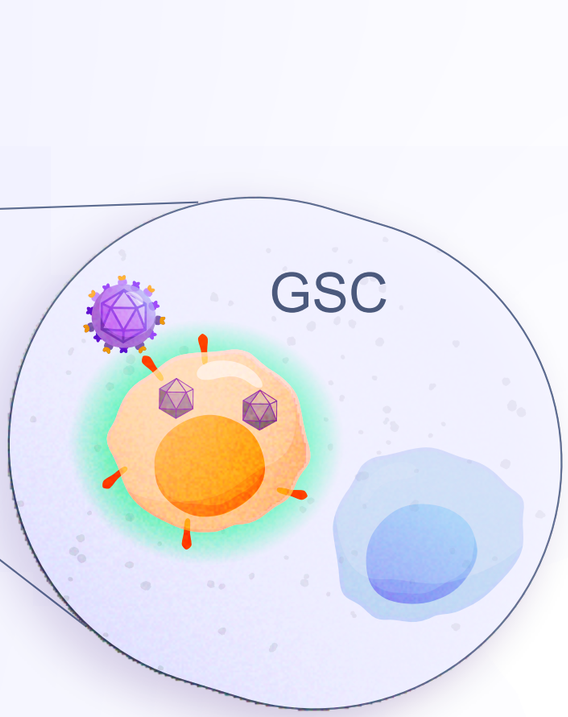

In vivo

PBS/Glycerol

CXCR4+ GBM mice

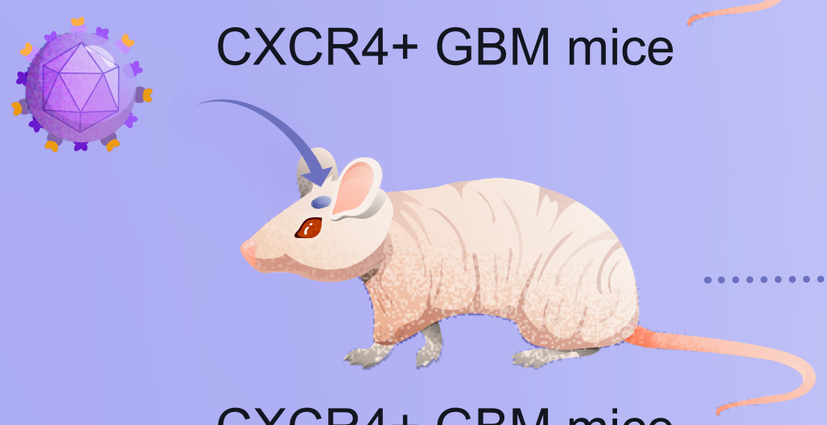

CXCR4+ GBM mice

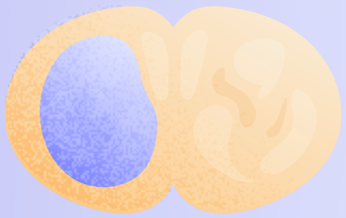

Brain section

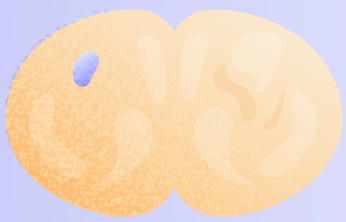

Brain section

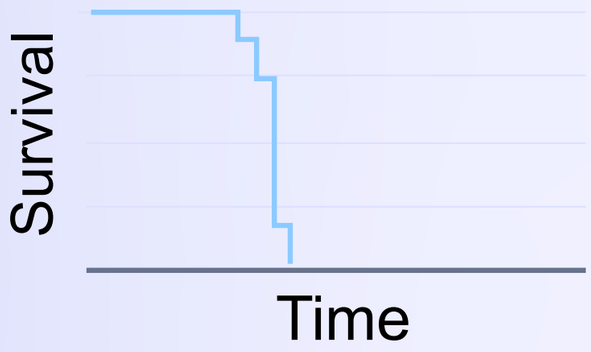

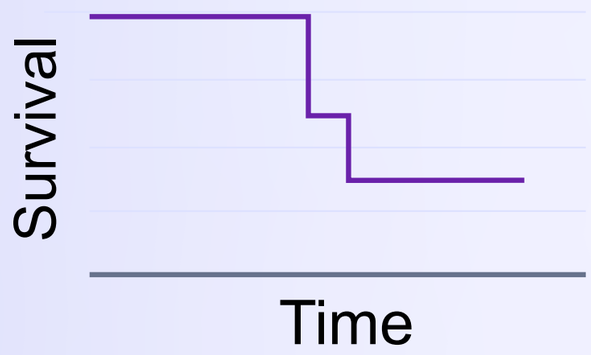

Nanobody-based retargeting of an oncolytic herpesvirus for eliminating CXCR4^{+} GBM cells: a proof-of-principle

Judit Sanchez Gil[1], Maxime Dubois[1], Virginie Neirinckx[2], Arnaud Lombard[2,3], Natacha Coppieters[2], Paolo D'Arrigo[1], Damla Isci[2], Therese Aldenhoff[2], Benoit Brouwers[2], Cédric Lassence[1], Bernard Rogister[2,4], Marielle Lebrun[1] and Catherine Sadzot-Delvaux[1].

[1] Laboratory of Virology, GIGA Infection, Inflammation and Immunity (GIGA I3), University of Liège, 4000 Liège, Belgium

[2] Laboratory of Nervous system Disorders and Therapy, GIGA-Neurosciences, University of Liège, 4000 Liège, Belgium

[3] Department of Neurosurgery, CHU of Liège, 4000 Liège, Belgium

[4] Department of Neurology, CHU of Liège, 4000 Liège, Belgium

Correspondence should be addressed to C.S-D, (csadzot@uliege.be), Laboratory of Virology and Immunology, GIGA I3, University of Liège, 11 Avenue de l'Hôpital, 4000 LIEGE, Belgium. Tel: +32 366 24 45

SHORT TITLE:

CXCR4^{+} GBM cell killing with a Nb-retargeted oHSV: a proof-of-principle

ABSTRACT

Glioblastoma (GBM) is the most aggressive primary brain tumor in adults, which remains difficult to cure. The very high recurrence rate has been partly attributed to the presence of glioblastoma stem-like cells (GSCs) within the tumors, which have been associated with elevated CXCR4 expression. CXCR4 is frequently overexpressed in cancer tissues, including GBM, and usually correlates with a poor prognosis. We have created a CXCR4-retargeted oncolytic herpesvirus (oHSV) by insertion of an anti-human CXCR4 nanobody in glycoprotein D of an attenuated HSV-1 (ΔICP34.5; ΔICP6; ΔICP47), thereby describing a proof-of-principle for the use of nanobodies to target oHSVs towards specific cellular entities. Moreover, this virus has been armed with a transgene expressing a soluble form of TRAIL to trigger apoptosis. *In vitro*, this oHSV infects U87MG CXCR4$^+$ and patient-derived GBM stem-like cells (GSCs) on a CXCR4-dependent manner and, when armed, triggers apoptosis. In a U87MG CXCR4$^+$ orthotopic xenograft mouse model, this oHSV slows down tumor growth and significantly improves mice survival. Customizing oHSVs with diverse nanobodies for targeting multiple proteins appears as an interesting approach for tackling the heterogeneity of GBM, especially GSCs. Altogether, our study must be considered as a proof-of-principle and a first step towards personalized GBM virotherapies to complement current treatments.

INTRODUCTION

The chemokine receptor 4 (CXCR4), first described for its role in leukocyte trafficking or HIV infection[1], is a largely studied G-protein-coupled receptor which activates various signaling pathways upon binding of its unique ligand CXCL12, also known as stromal cell-derived factor 1. CXCR4 overexpression has been reported in a wide range of tumors, including glioblastoma multiforme (GBM)[2–5] and increasing evidence has suggested its central role in cancer progression[6]. Multiple preclinical or clinical studies have demonstrated that the disruption of CXCR4 downstream signaling via several approaches (CXCR4 shRNA, CXCL12 mimetic peptide, anti-CXCR4 antibodies or nanobodies) diminishes tumor growth and synergizes with chemo- or radiotherapy[7–13]. GBM is the most frequent primary malignant brain tumor, classified by the World Health Organization as a grade 4 glioma[14]. Despite standard therapies that associate surgical resection with radio- or chemotherapy, the prognosis remains dramatically poor, with a median survival of 16 months from diagnosis[15]. GBM is indeed highly diffuse and tumor cells infiltrate healthy brain tissue, making the total resection of the tumor rather difficult or even impossible. GBM recurrences frequently develop within the margin of the resection cavity or at distant sites[16]. In addition, GBM is characterized by a high degree of heterogeneity at the genetic, epigenetic and transcriptomic levels. Many studies reported the presence of self-renewing, multipotent subsets of GBM cells endowed with high tumorigenic capacity, considered as GBM stem-like cells (GSCs)[17–19]. GSCs have been associated with the expression of specific markers, form tumorospheres *in vitro* upon limiting dilution, and are able to initiate a tumor when serially-transplanted in mice brain. GSCs have long been considered as key actors in GBM relapse, and the mechanisms underlying GSC development, maintenance and phenotypic plasticity yet remain intensively investigated[20]. We previously have shown that

upon GBM xenotransplantation, CXCR4$^+$ GSCs escape the tumor core and reach the subventricular zones (SVZ) based on a CXCR4/CXCL12-dependent signaling[21,22]. GSCs hosted in the SVZ display an improved DNA double-strand break repair, and hence are resistant to radiotherapy[22,23]. These observations have been confirmed in GBM patients, in which GSCs can be found both in the tumor core where the hypoxic environment constitutes an appropriate niche and in the SVZ, reinforcing the role of these CXCR4$^+$ cells in GBM recurrence[24,25]. Importantly, a high expression of CXCR4 positively correlates with tumor size, tumor progression, recurrence and ultimately with patient survival[3,5]. Targeting GSCs and particularly CXCR4$^+$ cells therefore provides an opportunity to reach tumor cells that escape current treatments[26].

Over the last decade, virotherapy has emerged as a promising approach for cancer treatment[27]. Oncolytic viruses (OV) are currently at different stages of preclinical investigations and numerous clinical trials are ongoing. In the context of GBM, virotherapy and oncolytic herpesviruses (oHSV) in particular are currently being evaluated as an alternative or complementary therapeutic approach for patients resistant to traditional therapies[28]. oHSV efficacy depends on the capacity of the virus to specifically infect cancer cells. However, it is estimated that about 20% of the GBM cells are not efficiently infected by oHSV partly due to a low expression of CD111 (Nectin 1, one of the HSV-1 natural receptors)[29,30]. A virus able to target cancer cells and, GSCs in particular, through its interaction with a membrane protein specifically expressed by these cells, would thus allow to reach cells that have escaped standard therapeutic approaches. One strategy for oHSV retargeting is to replace the domain responsible for glycoprotein D (gD) interaction with its natural cellular receptors by a ligand able to interact with a protein of interest expressed by the target cells. Single chain Immuno-

globulin (scFv) or ligands such as cytokines or peptides have been successfully introduced in gD to target cancer cells[31–36]. Nanobodies are single heavy variable domain of camelid antibodies and constitute an interesting alternative to retarget an oHSV. They can be selected from a synthetic or immune library with a huge diversity and can recognize cryptic antigens with a high affinity. These nanobodies therefore open the possibility to develop a panel of tailored oHSVs for personalized therapy.

In this context, we have developed, as a proof-of-principle, an oncolytic HSV-1 specifically targeting CXCR4, thanks to the insertion in gD of an anti-human CXCR4 nanobody previously described for its capacity to efficiently recognize CXCR4 (WO 2016/156570 Al). This virus (oHSV/Nb-gD) has been further armed with a transgene expressing the soluble form of TRAIL (oHSV/Nb-gD:sTRAIL), whose efficacy to trigger the extrinsic apoptosis pathway has been previously documented[37–40]. We demonstrated that the engineered virus infects U87MG CXCR4$^+$ and patient-derived GSCs in a CXCR4-dependent manner, can replicate efficiently in these cells and lead to sTRAIL expression, thereby triggering apoptosis. When used in an *in vivo* orthotopic xenograft GBM model, oHSV/Nb-gD armed or not with sTRAIL had a clear impact on tumor progression and significantly improved mice survival. These results confirm nanobodies as appropriate tools for retargeting oHSVs towards specific cell subsets and constitute a proof-of-principle of an oHSV design strategy that could be considered for personalized treatment.

RESULTS

Construction of a nanobody-retargeted and armed oncolytic herpesvirus

To specifically target GBM cells expressing CXCR4, we engineered an oHSV that was first detargeted from its natural receptors HVEM and nectin-1, prior to being retargeted to CXCR4 (Figure 1). These modifications were introduced within fQuick-1 (kind gift from Prof. EA. Chiocca), a BAC containing the HSV-1 genome (Strain F; ΔICP34.5/ ΔICP6/EGFP^{+}). This backbone was further deleted from US12 coding for ICP47, this deletion being important to partly overcome the attenuation resulting from γ34.5 deletion[41]. The detargeting/retargeting was achieved by replacing the residues 2-24 of gD, within the HVEM-binding domain by an anti-human CXCR4 nanobody[42]. In addition, the residue 38 of gD was mutated (Y38C) to impair gD interaction with nectin-1, another natural receptor[43]. Moreover, two mutations (D285N and A549T) shown to improve the fusion capacity of glycoprotein B (gB) were introduced in UL27[44]. Finally, the virus was armed with a transgene expressing a soluble form of TRAIL (sTRAIL)[45] under the control of a nestin promoter. After transfection of these constructs into VERO cells previously transduced with the human CXCR4, oHSVs were produced in the supernatant, and further purified and titrated. In this publication, they are referred to as oHSV/gD (non-retargeted; non-armed), oHSV/Nb-gD (CXCR4-retargeted; non-armed), oHSV/Nb-gD:sTRAIL (CXCR4-retargeted and sTRAIL-armed).

Efficacy of the CXCR4-retargeting.

To verify the detargeting efficacy, J1.1-2, hamster cells resistant to HSV due to the lack of HVEM or nectin-1 expression at the cell surface[46], as well as their modified version J/A and J/C expressing respectively human HVEM[47] or nectin-1[48] (kind gift from Pr. G. Campadelli Fiume), were infected with oHSV/gD or oHSV/Nb-gD (MOI: 0.01; 0.1 and 1). Contrary to oHSV/gD which led to numerous infectious foci in J/A and

J/C, no foci were detected upon oHSV/Nb-gD infection, demonstrating that oHSV/Nb-gD was properly detargeted (Figure 2A). To evaluate the capacity of oHSV/Nb-gD to specifically infect CXCR4$^+$ cells, glioblastoma U87MG cells which express CXCR4 at a very low level (Figures S1A and B) were transduced with a lentivirus expressing the human CXCR4. The ectopic expression of CXCR4 was confirmed by flow cytometry (Figures S1A and B). U87MG and U87MG CXCR4$^+$ were infected with oHSV/gD or oHSV/Nb-gD (MOI: 0.1) and the level of infection was evaluated by real-time GFP imaging and quantification with Incucyte® S3 (Figures 2B, C and S2). As expected, oHSV/gD efficiently replicated in both cell lines independently of CXCR4 expression. On the contrary, oHSV/Nb-gD infection remained very low in U87MG cells with only very few cells infected as reflected by a very weak eGFP expression and no statistical difference with the non-infected cells. This clearly contrasted with numerous foci and overtime increasing eGFP signal in oHSV/Nb-gD-infected U87MG CXCR4$^+$ cells, confirming that oHSV/Nb-gD infection relies on the expression of CXCR4. Importantly, the efficacy of infection of oHSV/gD and oHSV/Nb-gD in U87MG CXCR4$^+$ cells was similar. This was further confirmed by This was further confirmed by a growing curve of both oHSVs in U87MG-CXCR4$^+$ cells. No statistical difference was observed (Figure S3).

CXCR4-dependent infection of patient-derived GSCs by oHSV/Nb-gD.

The efficacy of oHSV/gD and oHSV/Nb-gD was further evaluated on four different GBM stem-like cells cultures (T08, T013, T018 and T033) directly established from residual GBM tissue obtained from surgical resection (Department of Neurosurgery, CHU Liège, Belgium) and maintained as tumorospheres. In opposition to U87MG cells, GSCs express high levels of *SOX2*, *POU3F2* and *SALL2* (Figure S4). The percentage of CXCR4$^+$ cells among the four different GSC cultures analyzed by flow cytometry

was highly variable (Figures 3A and B). While less than 3% of T08 cells were positive for CXCR4, around 75% of T033 expressed this chemokine receptor, T013 and T018 being intermediate. As expected, the endogenous expression of CXCR4 was much lower than the ectopic expression by U87MG CXCR4^{+} cells (Figures 3 A and B). To evaluate the efficacy of the retargeted oHSV and to compare it with the non-retargeted virus efficacy, primary GSCs were cultured as tumorospheres and infected with oHSV/gD or oHSV/Nb-gD (10^6 PFU/ml). Forty-eight hours post-infection, cells were dissociated and the percentage of eGFP positive cells was analyzed by flow cytometry. Interestingly, the percentage of oHSV/Nb-gD infected cells clearly reflected the level of CXCR4 expression (Figure 3C). T033 which express CXCR4 at a high level were the most infected (34.8% of eGFP cells on an average, 48hpi) while less than 2% of T08 cells which do not express CXCR4 or express it at a very low level, were positive for eGFP. As expected, in most primary cells, oHSV/gD led to a higher percentage of infected cells compared to oHSV/Nb-gD (Figures 3C and S5). However, an Incucyte® S5 overtime analysis of T033 cells infected with a high titer (10^7/ml) indicated that both the dynamics and the eGFP fluorescence were similar for both viruses (Figure S6). Finally, it is worth mentioning that although all primary cell lines were infected by the non-retargeted virus, its efficacy greatly varied with T013 being significantly less infected than the other cell lines.

In parallel, tumorospheres were infected with oHSV/Nb-gD (10^6 PFU/ml) for immunostainings. Forty-eight hours post-infection, epifluorescence observation of oHSV infected tumorospheres revealed that eGFP intensity was very low in T08 and much brighter in T033, confirming that the level of infection reflects the level of CXCR4 expression (Figure 3D, left panels). Tumorospheres were then fixed for immunostainings. Confocal microscopy of oHSV/Nb-gD infected tumorospheres sections confirmed that

only very few T08 cells were eGFP$^+$ while more infected cells were observed in T013, T018 and T033 tumorospheres (Figure 3D). Although no clear co-localization between GFP and CXCR4 was observed at the cellular level, infected cells were usually observed in the CXCR4$^+$ area.

***In vitro* evaluation of the efficacy of the sTRAIL-arming.**

oHSV/Nb-gD, shown to be efficiently retargeted and to specifically infect CXCR4$^+$ cells was further armed with the gene coding for the soluble form of TRAIL under the control of the nestin promoter to trigger apoptosis upon viral infection. First, we showed that the armed- and non-armed oHSVs replicated with the same efficacy in VERO CXCR4$^+$ (data not shown) or U87MG CXCR4$^+$ cells (Figure 4A), demonstrating that the arming does not impair oHSV replication. The efficacy of sTRAIL to trigger the apoptosis pathway was analyzed either by western blotting or using an annexin V/DAPI assay, while the viability was evaluated by measuring the cellular metabolism with resazurin. The expression of sTRAIL upon infection of U87MG CXCR4$^+$ by oHSV/Nb-gD:sTRAIL led to the cleavage of PARP and caspase 3, while no cleavage was observed upon oHSV/Nb-gD infection (Figure 4B). The annexin V/DAPI assay further confirmed apoptosis in oHSV infected U87MG CXCR4$^+$ cells. sTRAIL-induced apoptosis was detectable at 48hpi and reached significance only at 72hpi with an average of 36% of apoptotic cells upon oHSV/Nb-gD:sTRAIL infection compared to 12% upon oHSV/Nb-gD infection (Figure 4C). At 72hpi, the percentage of apoptotic cells upon oHSV/Nb-gD:sTRAIL infection increased according to the MOI which was not the case with the non-armed oHSV (Figure S7). Interestingly, the viability of the cells infected by oHSV/Nb-gD or oHDSV/Nb-gD:sTRAIL measured 24, 48h or 72hpi was not statistically different (Figure 4C).

When used to infect patient-derived GSCs tumorospheres, oHSV/Nb-gD:sTRAIL led to the expression of gD and sTRAIL as measured by RT-qPCR and this expression was significantly higher in T033 tumorospheres (Figures 4D and E).

Evaluation of the therapeutic efficacy of oHSV/Nb-gD and oHSV/Nb-gD:sTRAIL using an orthotopic xenograft GBM model

The capacity of oHSV/Nb-gD and oHSV/Nb-gD:sTRAIL to impact tumor growth was evaluated *in vivo*, using an orthotopic xenograft GBM mouse model. A first experiment was set up with engraftment of $5x10^4$ U87MG $CXCR4^+Luc^+$ into the right striatum under stereotactic control (Figure S8A). PBS or oHSVs (1.4×10^6 PFU in 2 µl) were injected within the tumor on day 16. Weekly bioluminescence analysis revealed a very rapid tumor growth in all groups even beyond oHSV intratumoral injection, although tumor growth appeared slightly reduced in oHSV/Nb-gD or oHSV/Nb-gD:sTRAIL treated mice compared to PBS-treated mice (Figure S8B). From day 19 on, PBS-treated mice health status rapidly evolved towards a critical point that justified sacrifice on day 24 (Figure S8C). Although not conclusive, these results paved the way for the design of another experiment, in which PBS or oHSVs (1.4×10^6 PFU in 2µl) were injected on day 7 after engraftment of $5x10^4$ U87MG $CXCR4^+Luc^+$ GBM· cells (Figure 5A). Body weight was monitored every second day, and bioluminescence recording was performed weekly to evaluate the tumor size evolution. On day 22, mice were anesthetized and either perfused with saline solution only (for RNA extraction from brain tissue) or followed by paraformaldehyde to allow immunostaining analyses. Contrary to oHSV-treated mice which, temporary lost weight just after virus infection but showed a continuous weight gain until the end of the experiment, PBS-treated mice displayed a clear weight loss from day 20 on (Figure 5B). On day 6, the tumor size appeared homoge-

neous among groups, with no significant difference in the bioluminescent signal (Figures 5C and S9A). On day 13, bioluminescence in PBS-treated mice dramatically increased up to day 20, whereas the signal in oHSV-treated mice remained similar to day 6 or even decreased, becoming even undetectable in some mice (Figure 5C). All mice were sacrificed on day 22 and brains were harvested for either anti-human vimentin immunohistochemical staining and tumor size measurement (5 mice/group) or RNA extraction and RT-qPCR analyses (4 mice/group). The size of the tumor, calculated by measuring the area positive for human vimentin on serial sections and 3D volume reconstruction, clearly showed a significant impact of both oHSV/Nb-gD and oHSV/Nb-gD:sTRAIL treatment, even if no significant difference was observed between the two viruses (Figures 5D and E). For RNA extraction, right hemispheres, in which the cells were engrafted, were divided into three parts (frontal, middle, and occipital). Human CXCR4 expression, reflecting the presence of implanted human $CXCR4^+$ GBM cells, was evaluated in each block individually and expressed as the relative expression to the level of expression in the middle part of PBS-treated mice brains (Figure 5F). Overall, human CXCR4 expression was significantly decreased in oHSV-treated mice compared to PBS-treated mice. In both oHSV-treated groups, differences in the level of expression of hCXCR4 were observed between the 3 blocks, with a higher abundance of human transcripts detected in samples corresponding to the frontal and middle samples, covering the initial site of engraftment. These results were confirmed by RT-qPCR for human nestin and TBP (data not shown) and corroborated bioluminescence analyses that showed some signal, although quite low in oHSV-treated mice (Figure S9A). At the end of the experiment (15 days after virus injection), we were unable to detect gD or sTRAIL neither by immunohistochemistry nor by RT-qPCR (data not shown).

To verify whether, *in vivo,* oHSVs effectively replicate in tumor cells and sTRAIL is expressed, this experiment was repeated with the same settings, but mice were sacrificed two days after virus injection. Right hemispheres were divided into three parts (frontal, middle, and occipital) and total RNA was extracted from the brain tissue. gD and sTRAIL relative expression measured by RT-qPCR demonstrated the presence of gD transcripts in brains injected with oHSV/Nb-gD and oHSV/Nb-gD:sTRAIL while sTRAIL transcripts were detected only in the oHSV/Nb-gD:sTRAIL group (Figures S9B and C). Finally, a survival assay was set up with similar experimental settings (Figure 6A). U87MG $CXCR4^{+}Luc^{+}$ cells were injected under stereotactic control. All mice developed tumors (Figure S10A) and viral suspension, or PBS was injected within the tumor on day 7. Body weight was monitored every second day and mice were sacrificed when showing a significant weight loss or severe clinical signs. From day 19, all PBS-treated mice continuously lost weight, while oHSV-treated mice started to lose weight only on day 29, with the mice still alive 35 days after infection continuing to gain weight (Figure S10B). Again, tumor size appeared similar in all groups just before (day 5) virus injection (Figures 6B and S10A). However, one week after the intratumoral injection (day 13), bioluminescence signal in oHSV-treated mice was significantly reduced compared to the PBS group. In these oHSV-injected tumors, bioluminescence was very low and even undetectable in 4/6 and 3/5 mice in oHSV/Nb-gD and oHSV/Nb-gD:sTRAIL, respectively (Figures 6B and S10A). However, no significant difference was observed between oHSV/Nb-gD and oHSV/Nb-gD:sTRAIL-treated mice (Figure 6B). Importantly, while all PBS-treated mice died between day 21 and 27, the oHSV-treated mice death was significantly delayed with the first deaths observed on day 31 (Figure 6C). At day 61, 1/6 oHSV/Nb-gD and 2/5 oHSV/Nb-gD:sTRAIL treated mice were still alive. Taken together, all these results show that oHSV/Nb-gD and oHSV/Nb-

gD:sTRAIL are suited for intratumoral injection in GBM orthotopic models and exert a potent oncolytic activity *in vivo*.

DISCUSSION

Glioblastoma (GBM) remains the most aggressive form of adult brain cancer, associated to a dismal prognosis. Therapeutic failure and high recurrence rate endorse the need for novel, alternative, or add-on approaches to improve the standard-of-care therapy. GBM exhibits a wide cellular diversity, with malignant cells being highly heterogeneous in terms of molecular profile, phenotype, tumorigenic potential and resistance to treatment. Such heterogeneity is largely accountable for tumor recurrence.

A subset of GBM cells considered as stem-like cells (GSCs) display stemness features, appear more resistant to radio- and chemotherapies and are endowed with increased tumorigenicity[49]. Targeting GSCs thus appears as an opportunity for new therapeutic approaches. A wide variety of therapeutic strategies aiming to target GSCs have been evaluated in preclinical models and are being clinically translated[26]. However, considering the biological complexity and phenotypic plasticity of those cells, the main hurdle is to target GSCs without impairing normal tissue. In the perspective of eradicating peculiar GBM cell entities such as GSCs, highly specific and targeted strategies should be considered.

Oncolytic virotherapy has been proposed as a promising avenue for GBM therapy, and herpesviruses offer numerous opportunities for tailored design and targeting strategies. oHSVs are the first viruses approved by the FDA for virotherapy. Their mechanism of cell entry is well documented[50], and can be modified to restrict oHSV entry into cells that specifically express a receptor of interest at their surface. oHSV retargeting requires the replacement of the viral glycoprotein domain important for their interaction with either the heparan sulfate or the natural receptors, by a ligand specific for a protein

of interest. Single-chain antibodies (scFv), cytokines or specific ligands have been described for their efficacy to retarget oHSV[31–35]. In our study, we describe oHSV retargeting using a nanobody. Nanobodies correspond to the single heavy variable domain of camelid antibodies. They can be quite easily obtained by screening either immune or artificial libraries characterized by a huge sequence diversity, and thereby constitute an interesting tool for oHSV customization and specific targeting.

In this study, GBM has been chosen as a model to evaluate the nanobody-based oHSV retargeting. As a proof-of-principle, we considered to genetically engineer an oHSV whose gD is modified by the insertion of a nanobody able to recognize hCXCR4, a chemokine receptor expressed on several GBM cell subtypes, including glioblastoma stem-like cells (GSCs). CXCR4 has been associated with cancer cell proliferation, tumorigenesis, migration and its expression correlates with a poor prognosis[51]. Additionally, we have previously shown $CXCR4^+$ cells as able to move away from the tumor core and specifically invade the subventricular zones[21], and targeting of CXCR4 therefore appears as an encouraging approach. The CXCR4-retargeted oHSV described in this paper (namely oHSV/Nb-gD) has been engineered from an attenuated backbone (ΔICP34.5, ΔICP6 and ΔICP47) whose safety in GBM treatment has been largely documented[41]. Other oHSVs retargeted to the Epidermal Growth Factor Receptor (EGFR), the human receptor tyrosine-protein kinase erbB-2 (hHER2), the interleukin 13 receptor, the epithelial cell adhesion molecule (EpCAM), or the urokinase Plasminogen Activator Receptor, all described to be overexpressed in cancer tissues have been constructed and characterized[31–36]. Contrarily to the oHSVs described in this paper, all these retargeted viruses were engineered in a non-attenuated HSV background, inducing a higher level of viral replication. However, their safety only relies on the tight control of their entry into cancer cells and consequently requires an absence or a very

low expression of the target of interest on healthy cells. Similarly, the CXCR4-retargeted oHSVs entry depends on the capacity of the virus to specifically interact with a receptor but its attenuated character limits its replication in non-cancer cells, improving its safety. We show that the CXCR4-retargeted virus (oHSV/Nb-gD) can specifically infect on a CXCR4-dependent manner, not only U87MG CXCR4$^+$ but also patient-derived GSCs, despite a much lower CXCR4 endogenous expression. *In vitro*, when armed with a secreted form of TRAIL (oHSV/Nb-gD:sTRAIL), this virus is able to trigger apoptosis. The replication of these oncolytic viruses in cells transduced with CXCR4 is not impaired nor by the retargeting or the arming. Importantly, when inoculated at high titers (10^7 PFU/ml) on primary GBM cells expressing a high level of endogenous CXCR4 (T033), both the retargeted and the non-retargeted virus show the same kinetics and the same efficacy of infection.

When used *in vivo* in an orthotopic xenograft model of GBM in which U87MG CXCR4$^+$ cells were engrafted, both sTRAIL-armed and non-armed oHSVs were able to limit the tumor progression and to significantly improve mice survival. Even though sTRAIL triggers apoptosis *in vitro*, its impact in the xenograft model seems to be limited. Contrarily to the sTRAIL-armed oHSV previously described in the literature and whose expression is driven by the HSV immediate early promoter IE4/5[37,40], sTRAIL expression in oHSV/Nb-gD:sTRAIL is driven by the nestin promoter. Although nestin is overexpressed in most GBM tumors[26], it might not be activated at the same level in all GBM cells and hence be too restrictive for an optimal expression of sTRAIL. Moreover, *in vitro*, the percentage of apoptotic cells as measured by flow cytometry, does not reflect the strong impact of oHSV infection on U87MG viability (Figure 4C). The oncolysis mediated by the virus itself may hide the sTRAIL-induced apoptosis when high MOI

are used[37,40]. The efficacy of the arming should be further evaluated *in vivo* in the xenograft model after engraftment of patient-derived GSCs. If needed, a stronger promoter should be considered to drive sTRAIL expression. U87MG CXCR4$^+$ cells engrafted in the xenograft model have a very rapid growth kinetics. Such a rapid growth can hamper the total elimination of the tumor after a single virus injection and could explain the regrowth observed in some mice. In this context, it would be worth evaluating the impact of repeated injections or of continuous delivery of the virus thanks to a mini-osmotic pump system[52]. In addition, the role of the tumor microenvironment and especially of the innate immune response should not be underestimated. oHSV virotherapy has been shown to rapidly activate natural killer (NK) cells which diminish the virotherapy efficacy[53] while adenovirus virotherapy has been shown to induce a phenotypic shift of macrophages from pro-tumoral M2-like toward the anti-tumoral and pro-inflammatory M1-like phenotype[54]. A deeper characterization of the tumor microenvironment upon virotherapy will provide important information that might help to improve the treatment.

An important issue that must be carefully studied when targeting tumor cells is the fact that healthy cells might express the target of interest and thus be infected by the oncolytic virus. Although in our study oHSVs are attenuated, this issue must be taken into consideration. CXCR4 is mainly expressed in the bone marrow or lymphoid tissues and poorly expressed in the brain (https://www.proteinatlas.org/ENSG00000121966-CXCR4). Taking into consideration that the oHSV is injected within the tumor, CXCR4 expression on non-tumoral cells in the vicinity of the tumor must however be considered. We recently analyzed chemokine receptors (among which CXCR4) expression in GBM based on publicly available patient-derived transcriptomic data, which shows that CXCR4 is expressed in malignant cells, in endothelial cells within the tumor as

well as on TAMs (tumor associated macrophages) and TIL (Tumor infiltrating lymphocytes)[55]. The capacity of the CXCR4-retargeted virus to infect and potentially destroy these cells, especially endothelial cells and M2-like macrophages, would certainly be of interest, still the benefit/risk balance has to be assessed very carefully. Unfortunately, the anti-hCXCR4 nanobody used in this study does not recognize the murine CXCR4 which limits the questions that could be addressed in the human GBM xenograft model. We are currently screening a nanobody library to identify nanobodies that recognize both the human and murine CXCR4 receptor. Such nanobodies would allow not only to address important issues such as the undesired targeting of healthy cells but also to evaluate the importance of the immune response and particularly of the adaptive immune response, this latest requiring a syngeneic GBM murine model.

Altogether, the results described in this proof-of-principle study show that the retargeting of oHSVs by the insertion of a nanobody appears highly encouraging and constitutes an interesting approach for the targeting of GBM cell subsets, e.g. GSCs, expressing specific proteins of interest. Our data support the idea that a set of nanobodies specific for diverse GSCs markers may be used to customize oHSVs that could be exploited as an add-on to complement the current standard-of-care therapeutic approaches.

MATERIAL and METHODS

Cell lines

VERO cells (ATCC, #CCL-81) and human glioblastoma U87MG (ATCC # HTB-14) cells were maintained in Dulbecco's modified Eagle minimal essential medium (DMEM, Lonza, Verviers, Belgium) supplemented with 10% fetal bovine serum (FBS). J1.1-2 cells are HSV-1 resistant baby hamster kidney cells lacking both HVEM and nectin-1, two natural HSV-1 receptors. J/A and J/C cells are J1.1 transduced with HVEM and nectin-1 respectively (kind gift of Pr. G. Campadelli-Fiume (University of Bologna, Italy). They were cultured with DMEM supplemented with 5% of FBS. J/A and J/C cells were treated with 400 μg/ml of G418 (Invivogen, Belgium). VERO CXCR4$^+$ and U87MG CXCR4$^+$ obtained by transduction of a lentivirus (Viral Vector platform, University of Liege) were treated with 20 ng/ml and 10 ng/ml of blasticidin, respectively. Primary GBM primary cultures (T08, T013, T018 and T033) were established from freshly resected human glioblastoma tissue obtained from GBM patients. They were cultured as tumorospheres in stem cell medium (DMEM/F-12 with GlutaMAX (Gibco) supplemented with B27 (1/50) without vitamin A (Gibco), 1% Penicillin-streptomycin (Lonza, Verviers, Belgium), 1 μg/ml of heparin (n 7692.1, Carl Roth, Belgium), human EGF (20 ng/ml) and βFGF (20 ng/ml) (Peprotech).

Construction of recombinant oHSVs.

Recombinant viruses were engineered in fHsvQuik-1 Bacterial artificial chromosome (BAC) containing an attenuated strain F HSV-1 (Δγ34.5, ΔUL39, GFP$^+$; kind gift from A. Chiocca from the University of Pittsburg, USA). Recombinants were obtained by the two-step Red recombination technique "en passant" [56]. ICP47 deletion was done as described by Todo T *et al*., 2001[57]. The detargeting of gD from its naturals receptors

was performed according to Uchida *et al*, 2012[43]. For retargeting, we inserted a patented sequence coding for a nanobody against human CXCR4 receptor (CXCR4-NB; WO 2016/156570 Al) in the gD coding sequence. The “arming” sequence containing a soluble form of TRAIL (sTRAIL) [45] under the nestin promoter was inserted before the ICP6 promoter as shown in Figure 1. A double mutation (D285N and A549T) was inserted within gB to compensate the loss of infectivity generally observed upon gD retargeting [44]. CXCR4$^+$ Vero cells were plated in 6 well-plate at 40% confluence and transfected with 3 µg of BAC using JETPEI (Polyplus, Illkirch – FRANCE). Viral replication was detected 48h after transfection by the visualization of fluorescent foci. Virus stocks were produced and concentrated as previously described [58]. Briefly, cells were infected at low MOI (0.005) and cultured for four to five days at 33°C. The day before the experiment, cells were treated with 0,45 M of NaCl and 100 ug/ml of dextran sulfate. Supernatant was collected and centrifuged at 2200 g for 10 min at 4°C, then filtered with 0.8 µm filter to discard cell debris. Then, viral particles were ultracentrifugated at 47.850g at 4°C using Beckman SW27 rotor. Centrifugated virus was resuspended in PBS with 10% glycerol, aliquoted and stored at -80°C. Plaque assay in VERO CXCR4+ was used to titrate the virus and determine the amount of PFU/ml [59].

Viral growth assay

U87MG CXCR4$^+$ or VERO CXCR4$^+$ cells were seeded in a 12-well plate and infected with oHSV/gD, oHSV/Nb-gD or oHSV/Nb-gD:sTRAIL at a MOI of 1 for 24, 48 or 72h. Supernatant was then harvested and titer (PFU/ml) was determined by plaque assay as previously described [59]. The number of foci was calculated based on Incucyte® S3 imaging.

Entry assay

J1.1-2, J/A and J/C cells were seeded in a 24 well-plate the day before infection. Cells were infected with a MOI of 1, 0.1 and 0.01. After 48h, cells were fixed with 4% paraformaldehyde and washed with PBS. Images were collected with the Incucyte® S3 (Sartorius).

RT-qPCR

Total RNA was isolated using the RNA isolation Nucleospin® kit (Macherey-Nagel) according to the manufacturer's protocol. 500 ng of RNA were reverse transcribed using RevertAid H Minus First Strand cDNA Synthesis Kit (Thermo Scientific) with Random primers (for gD or sTRAIL transcripts detection) or oligo-dT primers (for stemness markers transcripts detection). TBP or 18S were used as controls. RT-qPCR reaction samples were prepared as follows: 4 µl of the diluted cDNA (2.5 ng in total for gD and sTRAIL or 10ng in total for stemness markers) were mixed with 5 µl of SYBR green (TAKYON, Eurogentec, Liege, Belgium) and 100 µM of primers in a final volume of 10 µl. Primers used for transcripts detection are described in Table 1. Quantitative realtime PCR was done using the Roche LightCycler 480 (3 min. at 95°C of activation; 45 cycles: Denaturation 95°C, 3 sec, Hybridization and Elongation 60°C 25 sec).

Flow cytometry

For CXCR4 detection by Flow Cytometry, cells were plated in 6 well-plate two days before analysis or cultured as tumorospheres. Tumorospheres and cells cultured as monolayers were washed with PBS and dissociated by incubating the cells for 10 min at 37°C with Accutase (Biowest, Nuaillé, France). Dissociated cells were centrifugated at 350g for 5 min at 4°C and washed with Flow Buffer (PBS with BSA 1%, EDTA 1mM and Azide 0,1 %). 5 µl of APC-conjugated anti-CXCR4 antibody (Biolegend, Amsterdam, The Nertherlands) were added to $1x10^5$ cells in 100µl of Flow buffer (dilution

1/20) and kept at 4°C for 1 hour in the dark. Cells were washed by adding 1 ml of Flow Buffer and centrifugated at 400g for 4 min at 4°C. After a second wash, cells were resuspended in 200 µl of Flow buffer and directly analyzed with the FACS CANTO II (BD biosciences). Data were analyzed with FlowJo software.

Annexin/DAPI assay

For Annexin V/DAPI apoptosis assay, 92.000 cells were seeded in a 12-well plate and infected with a MOI of 1, 5 or 10 for 72 hours. Cells were collected and resuspended in 140 µl of 1X Binding Buffer (Ref. 556454, BD Pharmingen,). Ten µl of DAPI (Invitrogen, 1:100) and 5µl of Annexin V-PE (Ref. AB 2869071, BD Biosciences,) were added and cells were incubated for 15 min at RT in the dark. Finally, 200 µl of 1X Binding buffer was added and samples were directly analyzed with the FACS FORTESSA^{TM} (BD biosciences). Data were analyzed with FlowJo software.

Viability assay

U87MG and U87MG CXCR4^{+} cells were plated in a 12-well plate and infected with the different viruses at a MOI of 5. Measure of viability was done at 24, 48 and 72h post infection by evaluating the metabolic activity using a Resazurin assay. At each time point, media was removed and replaced by 500 µL of resazurin (20% (v/v) in DMEM-10% FBS) and cells were further incubated for 4h at 37°C. Metabolized media was transferred into a 96-well flat-bottom black plate and read (λ ex= 535 nm; λ em=595 nm) using the multi-mode microplate reader (FilterMax F5). Results are expressed as a percentage of the control.

Real time measure of the GFP fluorescence.

U87MG and U87MG CXCR4+ cells were plated in 24 flat bottom plate (46.000 cells/well). After 24 hours of monolayer culture, cells were infected with oHSV/gD or oHSV/Nb-gD

(MOI: 0.1) and incubated in the Incucyte®S3 for real-time analyses of the mean eGFP fluorescence intensity with the whole well module (Magnification 4X).

Patient-derived GSCs cells were seeded in 96 round bottom plate (10.0000 cells/well) in stem cell medium. Twenty-four hours after seeding, tumorospheres were infected with oHSV/gD or oHSV/Nb-gD (10^4PFU/well) and incubated in the Incucyte ® S5 for a real-time analysis of the mean eGFP fluorescence intensity with the organoid module (Magnification 4X).

Immunofluorescence staining on tumorospheres

Tumorospheres were infected with 10^6 PFU/ml. Forty-eight hours post-infection (hpi), cells were washed and fixed with 4% paraformaldehyde for 20 minutes (min) and incubated overnight with 20% PBS-sucrose before being embedded with colored OCT (Neg-50™). Spheroids were cut into 5 µm-thick cryosections (Microm HM 560, Thermoscientific) and placed onto SuperFrost slides (Thermo Scientific). Sections were permeabilized with 0.3% Triton X-100 PBS solution for 10 min and unspecific binding sites were blocked with 5% BSA for 30 min. Tumorospheres sections were incubated overnight at 4°C with primary antibodies diluted in 5% BSA (rabbit anti-CXCR4 (Ref. AB124824, Abcam, 1:200); mouse anti-nestin (Ref. sc-23927, Santa Cruz, 1:250). After two washes, slides were incubated for 1h at RT in the dark with secondary antibodies (goat anti-mouse Alexa fluor 633 and goat anti-rabbit Alexa fluor 568, 1:500). Nuclei were stained by incubation with Hoechst for 10 min at 1:50000. Finally, Mowiol (Sigma) was added, and sections were covered by a coverslip. Staining was analyzed with Nikon A1R confocal microscope. Figures were composed and examined with ImageJ software.

Western-Blot assay

Cells were lysed with RIPA modified buffer (50mM of Tris-HCl, 150mM of NaCl, 1mM of EDTA, 1% NP40 and 0,25% of DOC). 80 µg of proteins were loaded on a 6 (for PARP and gD detection) or 12% (for caspase 3 and a-tubulin detection) SDS-acrylamide gel. After electrophoresis, proteins were transferred on a PVDF membrane (GE Healthcare) according to standard protocols. Mouse anti-gD was used to determine viral infection level (Ref. sc-21719, Santa Cruz, 1:1000), rabbit anti-PARP (Ref. 9532, Cell Signaling, 1:1000) and mouse anti-caspase 3 (CC3) (Ref. ALX-804-305, Enzo, Life Sciences, Brussels, Belgium, 1:1000,) were used to detect the activation of the apoptotic pathway. Mouse anti-alpha-tubulin (Ref. T6199, Sigma, 1:2000) was used as loading control. HRP-conjugated-anti-rabbit-IgG (Ref. 7074, Cell Signaling) and HRP-conjugated anti-mouse-IgG (Ref. 7076, Cell Signaling) were used as secondary antibodies. Signals were revealed using ECL and imaged with LAS4000 CCD camera (GE Healthcare).

In vivo experiments

Adult 6 weeks female immunodeficient Crl:NU-Foxn1nu mice (Charles River Laboratories, Brussels, Belgium) were used for xenograft experiments. The athymic nude mice were housed in sterilized, filter-topped cages the Animal Facility at the University of Liège and all experiments were performed as previously approved by the Animal Ethical Committee of the University of Liège, in accordance with the Declaration of Helsinki and following the guidelines of the Belgium Ministry of Agriculture in agreement with European Commission Laboratory Animal Care and Use Regulation. Intrastriatal grafts were performed following the previously described procedures [60]. Briefly, 50.000 U87MG $CXCR4^{+}Luc^{+}$ cells resuspended in 2 µl of PBS were injected into the right striatum of mice previously anesthetized with an intraperitoneal injection of a Rompun (Sedativum 2%, Bayer, Brussels, Belgium) and Ketalar (Ketamin 50

552 mg/mL, Pfizer, Brussels, Belgium) solution (V/V) prepared just before injection. Injec-
553 tion was performed according to stereotactic coordinates (0.5 mm anterior and 2.5 mm
554 lateral from the bregma and at a depth of 3 mm), allowing a precise and reproducible
555 injection site. Later, oncolytic viruses resuspended in 2 µl of PBS were injected, under
556 similar anesthesia, within the tumor using the same stereotactic coordinates. Mice
557 health status was evaluated daily, and mice were weighed regularly.

558 **Bioluminescence activity**

559 Immunodeficient nude mice bearing intracranial U87MG CXCR4^{+}Luc^{+} xenografts were
560 injected intraperitoneally with Beetle Luciferin Potassium salt (Ref. E1605, Promega)
561 (150 mg/kg). Under anesthesia using 2.5% isoflurane, mice were imaged with camera-
562 based bioluminescence imaging system (Xenogen IVIS 50®; exposure time 1 min, 15
563 min after intraperitoneal injection). Regions of interest were defined manually, and im-
564 ages were processed using Living Image and IgorPro Software (Version 2.60.1). Raw
565 data were expressed as total counts/sec or total counts/min.

566 **Brain tissue processing and tumor volume measurement**

567 Mice were euthanized with i.p. injection of Euthasol Vet (140 mg/kg) and intracardiac
568 perfusion of ice-cold saline solution, followed by paraformaldehyde 4% in PBS (for
569 histology). Brains were extracted, placed in sucrose 30% for tissue cryopreservation,
570 and sectioned into 14 µm-thick serial sections using a cryostat. Tumor volume analysis
571 was performed by immunohistochemistry for human vimentin detection (Mouse anti-
572 human vimentin, MAB3400, Merck, 1:200) with Polyview®Plus HRP-DAB kit (Enzo
573 Life Sciences, Brussels, Belgium). Tumor was delineated based on anti-vimentin pos-

574 itivity. 10 to 12 serial brain sections were analyzed using the Mercator software (Ex-
575 ploraNova, La Rochelle, France). 3D reconstitution and extrapolation of tumor volume
576 were performed using Map3D software.

577 **Statistical analysis**

578 All statistical analyses were performed using GraphPad Prism 9. Data are displayed
579 as Mean ± SEM. Depending on the experiments, paired *t*-Test, Krustall-Wallis or two-
580 way ANOVAs were performed as indicated in the figure legends. Statistical signifi-
581 cance of survival assay was analyzed by log-ranked (Mantel-Cox) test.

582
583

584

Acknowledgments

J.S-G and P.D. are respectively a Ph.D. student and a PhD funded by the TELEVIE-FNRS; M.D. is a Research Fellow of the FNRS-Belgium; A.L. is Clinical Post-doctoral Researcher of the FNRS-Belgium. This work was supported by grants from the National Fund for Scientific Research (FNRS, Télévie), the Special Funds of the University of Liège, the Leon Frédéricq Foundation, Liège, Belgium and the Neurological Foundation of New Zealand.

The authors would like to thank Adeline Deward for the graphical abstract and all the members of the GIGA Viral Vector, Imaging and Flow cytometry, Genomics platforms and animal facilities for valuable technical support.

Author contributions

Conception of the project: C.S-D.; Funding acquisition B.R. and C.S-D.; Design of the experiments: J.S-G., V.N., A.L., N.C., M.L, C.S-D; Experiments: J.S-G., D.I., M.D., P.D.; Technical assistance: C.L., T.A., B.B., Writing: C.S-D. and J.S-G.; Reviewing: P.D., V.N., B.R., A.L., M.L., N.C.

Data Availability Statement

All raw data are available upon request.

Declaration of interest

The authors declare no competing interests.

Keywords

Virotherapy; HSV; Glioblastoma; glioblastoma stem-like cells; GBM; GSC; Nanobody;

610 oncolytic herpesvirus; virus retargeting; CXCR4

REFERENCES

1. Feng, Y., Broder, C.C., Kennedy, P.E., and Berger, E.A. (1996). HIV-1 entry cofactor: Functional cDNA cloning of a seven-transmembrane, G protein-coupled receptor. Science (80). *272*, 872–877.
2. Alimohammadi, M., Rahimi, A., Faramarzi, F., Alizadeh-Navaei, R., and Rafiei, A. (2021). Overexpression of chemokine receptor CXCR4 predicts lymph node metastatic risk in patients with melanoma: A systematic review and meta-analysis. Cytokine *148*, 155691.
3. Salmaggi, A., Gelati, M., Pollo, B., Marras, C., Silvani, A., Balestrini, M.R., Eoli, M., Fariselli, L., Broggi, G., and Boiardi, A. (2005). CXCL12 expression is predictive of a shorter time to tumor progression in low-grade glioma: A single-institution study in 50 patients. J. Neurooncol. *74*, 287–293.
4. Katsumoto, K., and Kume, S. (2013). The role of CXCL12-CXCR4 signaling pathway in pancreatic development. Theranostics *3*, 11–17.
5. Gagliardi, F., Narayanan, A., Reni, M., Franzin, A., Mazza, E., Boari, N., Bailo, M., Zordan, P., and Mortini, P. (2014). The role of CXCR4 in highly malignant human gliomas biology: Current knowledge and future directions. Glia *62*, 1015–1023.
6. Santagata, S., Ieranò, C., Trotta, A.M., Capiluongo, A., Auletta, F., Guardascione, G., and Scala, S. (2021). CXCR4 and CXCR7 Signaling Pathways: A Focus on the Cross-Talk Between Cancer Cells and Tumor Microenvironment. Front. Oncol. *11:591386.*
7. Gagner, J.P., Sarfraz, Y., Ortenzi, V., Alotaibi, F.M., Chiriboga, L.A., Tayyib, A.T., Douglas, G.J., Chevalier, E., Romagnoli, B., Tuffin, G., et al. (2017). Multifaceted C-X-C Chemokine Receptor 4 (CXCR4) Inhibition Interferes with

636 Anti–Vascular Endothelial Growth Factor Therapy–Induced Glioma
637 Dissemination. Am. J. Pathol. *187*, 2080–2094.
638 8. Gatti, M., Pattarozzi, A., Bajetto, A., Würth, R., Daga, A., Fiaschi, P., Zona, G.,
639 Florio, T., and Barbieri, F. (2013). Inhibition of CXCL12/CXCR4
640 autocrine/paracrine loop reduces viability of human glioblastoma stem-like cells
641 affecting self-renewal activity. Toxicology *314*, 209–220.
642 9. Mercurio, L., Ajmone-Cat, M.A., Cecchetti, S., Ricci, A., Bozzuto, G., Molinari,
643 A., Manni, I., Pollo, B., Scala, S., Carpinelli, G., et al. (2016). Targeting CXCR4
644 by a selective peptide antagonist modulates tumor microenvironment and
645 microglia reactivity in a human glioblastoma model. J. Exp. Clin. Cancer Res.
646 *35*, 1–15.
647 10. Gil, M., Seshadri, M., Komorowski, M.P., Abrams, S.I., and Kozbor, D. (2013).
648 Targeting CXCL12/CXCR4 signaling with oncolytic virotherapy disrupts tumor
649 vasculature and inhibits breast cancer metastases. Proc. Natl. Acad. Sci. U. S.
650 A. *110*, E1291-300.
651 11. Scala, S. (2015). Molecular pathways: Targeting the CXCR4-CXCL12 Axis-
652 Untapped potential in the tumor microenvironment. Clin. Cancer Res. *21*, 4278–
653 4285.
654 12. Kioi, M., Vogel, H., Schultz, G., Hoffman, R.M., Harsh, G.R., and Brown, J.M.
655 (2010). Inhibition of vasculogenesis, but not angiogenesis, prevents the
656 recurrence of glioblastoma after irradiation in mice. J. Clin. Invest. *120*, 694–705.
657 13. Lee, C.C., Lai, J.H., Hueng, D.Y., Ma, H.I., Chung, Y.C., Sun, Y. yun, Tsai, Y.J.,
658 Wu, W. Ben, and Chen, C.L. (2013). Disrupting the CXCL12/CXCR4 axis
659 disturbs the characteristics of glioblastoma stem-like cells of rat RG2
660 glioblastoma. Cancer Cell Int. *13*, 85-96.

14. Ostrom, Q.T., Gittleman, H., Truitt, G., Boscia, A., Kruchko, C., and Barnholtz-Sloan, J.S. (2018). CBTRUS statistical report: Primary brain and other central nervous system tumors diagnosed in the United States in 2011-2015. Neuro. Oncol. *20*, 1-86.

15. Stupp, R., Taillibert, S., Kanner, A., Read, W., Steinberg, D.M., Lhermitte, B., Toms, S., Idbaih, A., Ahluwalia, M.S., Fink, K., et al. (2017). Effect of Tumor-Treating Fields Plus Maintenance Temozolomide vs Maintenance Temozolomide Alone on Survival in Patients With Glioblastoma: A Randomized Clinical Trial. JAMA *318*, 2306–2316.

16. Lara-Velazquez, M., Al-Kharboosh, R., Jeanneret, S., Vazquez-Ramos, C., Mahato, D., Tavanaiepour, D., Rahmathulla, G., and Quinone-Hinojosa, A. (2017). Advances in brain tumor surgery for glioblastoma in adults. Brain Sci. *7*, 166-182.

17. Singh, S.K., Hawkins, C., Clarke, I.D., Squire, J.A., Bayani, J., Hide, T., Henkelman, R.M., Cusimano, M.D., and Dirks, P.B. (2004). Identification of human brain tumour initiating cells. Nature *432*, 396–401.

18. Galli, R., Binda, E., Orfanelli, U., Cipelletti, B., Gritti, A., De Vitis, S., Fiocco, R., Foroni, C., Dimeco, F., and Vescovi, A. (2004). Isolation and characterization of tumorigenic, stem-like neural precursors from human glioblastoma. Cancer Res. *64*, 7011–7021.

19. Chen, R., Nishimura, M.C., Bumbaca, S.M., Kharbanda, S., Forrest, W.F., Kasman, I.M., Greve, J.M., Soriano, R.H., Gilmour, L.L., Rivers, C.S., et al. (2010). A Hierarchy of Self-Renewing Tumor-Initiating Cell Types in Glioblastoma. Cancer Cell *17*, 362–375.

20. Singh, S.K., Clarke, I.D., Terasaki, M., Bonn, V.E., Hawkins, C., Squire, J., and

686 Dirks, P.B. (2003). Identification of a cancer stem cell in human brain tumors.
687 Cancer Res. *63*, 5821–5828.
688 21. Goffart, N., Kroonen, J., Di Valentin, E., Dedobbeleer, M., Denne, A., Martinive,
689 P., and Rogister, B. (2015). Adult mouse subventricular zones stimulate
690 glioblastoma stem cells specific invasion through CXCL12/CXCR4 signaling.
691 Neuro. Oncol. *17*, 81–94.
692 22. Goffart, N., Lombard, A., Lallemand, F., Kroonen, J., Nassen, J., Di Valentin, E.,
693 Berendsen, S., Dedobbeleer, M., Willems, E., Robe, P., et al. (2017). CXCL12
694 mediates glioblastoma resistance to radiotherapy in the subventricular zone.
695 Neuro. Oncol. *19*, 66–77.
696 23. Dedobbeleer, M., Willems, E., Lambert, J., Lombard, A., Digregorio, M.,
697 Lumapat, P.N., Di Valentin, E., Freeman, S., Goffart, N., Scholtes, F., et al.
698 (2020). MKP1 phosphatase is recruited by CXCL12 in glioblastoma cells and
699 plays a role in DNA strand breaks repair. Carcinogenesis *41*, 417–429.
700 24. Cheray, M., Bégaud, G., Deluche, E., Nivet, A., Battu, S., Lalloué, F., Verdier,
701 M., and Bessette, B. (2017). Cancer Stem-Like Cells in Glioblastoma. In
702 Glioblastoma, Codon Publications, Brisbane, Australia, Chapter 4, 59–71.
703 25. Lombard, A., Digregorio, M., Delcamp, C., Rogister, B., Piette, C., and
704 Coppieters, N. (2021). The Subventricular Zone, a Hideout for Adult and
705 Pediatric High-Grade Glioma Stem Cells. Front. Oncol. *10,* 614930.
706 26. Tang, X., Zuo, C., Fang, P., Liu, G., Qiu, Y., Huang, Y., and Tang, R. (2021).
707 Targeting Glioblastoma Stem Cells: A Review on Biomarkers, Signal Pathways
708 and Targeted Therapy. Front. Oncol. *11:* 701291.
709 27. Fountzilas, C., Patel, S., and Mahalingam, D. (2017). Review: Oncolytic
710 virotherapy, updates and future directions. Oncotarget *8*, 102617–102639.

711 28. Miyauchi, J.T., and Tsirka, S.E. (2018). Advances in immunotherapeutic
712 research for glioma therapy. J. Neurol. *265*, 741–756.
713 29. Friedman, G.K., Langford, C.P., Coleman, J.M., Cassady, K.A., Parker, J.N.,
714 Markert, J.M., and Gillespie, G.Y. (2009). Engineered herpes simplex viruses
715 efficiently infect and kill CD133+ human glioma xenograft cells that express
716 CD111. J. Neurooncol *95*, 199–209.
717 30. Rueger, M.A., Winkeler, A., Miletic, H., Kaestle, C., Richter, R., Schneider, G.,
718 Hilker, R., Heneka, M.T., Ernestus, R.I., Hampl, J.A., et al. (2005). Variability in
719 infectivity of primary cell cultures of human brain tumors with HSV-1 amplicon
720 vectors. Gene Ther. *12*, 588–596.
721 31. Menotti, L., Nicoletti, G., Gatta, V., Croci, S., Landuzzi, L., De Giovanni, C.,
722 Nanni, P., Lollini, P.-L., and Campadelli-Fiume, G. (2009). Inhibition of human
723 tumor growth in mice by an oncolytic herpes simplex virus designed to target
724 solely HER-2-positive cells. Proc. Natl. Acad. Sci. U. S. A. *106*, 9039–44.
725 32. Kamiyama, H., Zhou, G., and Roizman, B. (2006). Herpes simplex virus 1
726 recombinant virions exhibiting the amino terminal fragment of urokinase-type
727 plasminogen activator can enter cells via the cognate receptor. Gene Ther. *13*,
728 621–629.
729 33. Zhou, G., and Roizman, B. (2006). Construction and properties of a herpes
730 simplex virus 1 designed to enter cells solely via the IL-13α2 receptor. Proc. Natl.
731 Acad. Sci. U. S. A. *103*, 5508–5513.
732 34. Grandi, P., Fernandez, J., Szentirmai, O., Carter, R., Gianni, D., Sena-Esteves,
733 M., and Breakefield, X.O. (2010). Targeting HSV-1 virions for specific binding to
734 epidermal growth factor receptor-vIII-bearing tumor cells. Cancer Gene Ther. *17*,
735 655–63.

35. Shibata, T., Uchida, H., Shiroyama, T., Okubo, Y., Suzuki, T., Ikeda, H., Yamaguchi, M., Miyagawa, Y., Fukuhara, T., Cohen, J.B., et al. (2016). Development of an oncolytic HSV vector fully retargeted specifically to cellular EpCAM for virus entry and cell-to-cell spread. Gene Ther. *23*, 479–488.

36. Alessandrini, F., Menotti, L., Avitabile, E., Appolloni, I., Ceresa, D., Marubbi, D., Campadelli-Fiume, G., and Malatesta, P. (2019). Eradication of glioblastoma by immuno-virotherapy with a retargeted oncolytic HSV in a preclinical model. Oncogene. *23,* 4467–4479.

37. Jahan, N., Lee, J.M., Shah, K., and Wakimoto, H. (2017). Therapeutic targeting of chemoresistant and recurrent glioblastoma stem cells with a proapoptotic variant of oncolytic herpes simplex virus. Int. J. cancer *141*, 1671–1681.

38. Kim, M.-H., Billiar, T.R., and Seol, D.-W. (2004). The secretable form of trimeric TRAIL, a potent inducer of apoptosis. Biochem. Biophys. Res. Commun. *321*, 930–935.

39. Kock, N., Kasmieh, R., Weissledery, R., and Shah, K. (2007). Tumor therapy mediated by lentiviral expression of shBcl-2 and S-TRAIL1. Neoplasia *9*, 435–442.

40. Tamura, K., Wakimoto, H., Agarwal, A.S., Rabkin, S.D., Bhere, D., Martuza, R.L., Kuroda, T., Kasmieh, R., and Shah, K. (2013). Multimechanistic tumor targeted oncolytic virus overcomes resistance in brain tumors. Mol. Ther. *21*, 68–77.

41. Wakimoto, H., Kesari, S., Farrell, C.J., Curry, W.T., Zaupa, C., Aghi, M., Kuroda, T., Stemmer-Rachamimov, A., Shah, K., Liu, T.C., et al. (2009). Human glioblastoma-derived cancer stem cells: Establishment of invasive glioma models and treatment with oncolytic herpes simplex virus vectors. Cancer Res.

69, 3472–3481.

42. US20170362314A1 - Anti-CXCL12 Antibody Molecules and Their Uses - Google Patents.

43. Uchida, H., Marzulli, M., Nakano, K., Goins, W.F., Chan, J., Hong, C.-S., Mazzacurati, L., Yoo, J.Y., Haseley, A., Nakashima, H., et al. (2013). Effective treatment of an orthotopic xenograft model of human glioblastoma using an EGFR-retargeted oncolytic herpes simplex virus. Mol. Ther. *21*, 561–569.

44. Uchida, H., Chan, J., Goins, W.F., Grandi, P., Kumagai, I., Cohen, J.B., and Glorioso, J.C. (2010). A Double Mutation in Glycoprotein gB Compensates for Ineffective gD-Dependent Initiation of Herpes Simplex Virus Type 1 Infection. J. Virol. *84*, 12200–12209.

45. Shah, K., Tung, C.H., Yang, K., Weissleder, R., and Breakefield, X.O. (2004). Inducible Release of TRAIL Fusion Proteins from a Proapoptotic Form for Tumor Therapy. Cancer Res. *64*, 3236–3242.

46. Cocchi, F., Menotti, L., Mirandola, P., Lopez, M., and Campadelli-Fiume, G. (1998). The Ectodomain of a Novel Member of the Immunoglobulin Subfamily Related to the Poliovirus Receptor Has the Attributes of a Bona Fide Receptor for Herpes Simplex Virus Types 1 and 2 in Human Cells. J. Virol. *72*, 9992–10002.

47. Uchida, H., Shah, W.A., Ozuer, † Ali, Frampton, A.R., Goins, W.F., Grandi, P., Cohen, J.B., and Glorioso, J.C. (2009). Generation of Herpesvirus Entry Mediator (HVEM)-Restricted Herpes Simplex Virus Type 1 Mutant Viruses: Resistance of HVEM-Expressing Cells and Identification of Mutations That Rescue Nectin-1 Recognition. J. Virol. *83*, 2951–2961.

48. Frampton, A.R., Stolz, D.B., Uchida, H., Goins, W.F., Cohen, J.B., and Glorioso,

J.C. (2007). Equine Herpesvirus 1 Enters Cells by Two Different Pathways, and Infection Requires the Activation of the Cellular Kinase ROCK1. J. Virol. *81*, 10879–10889.

49. Lathia, J.D., Mack, S.C., Mulkearns-Hubert, E.E., Valentim, C.L.L., and Rich, J.N. (2015). Cancer stem cells in glioblastoma. Genes Dev. *29*, 1203–1217.

50. Connolly, S.A., Jardetzky, T.S., and Longnecker, R. (2021). The structural basis of herpesvirus entry. Nat. Rev. Microbiol. *19*, 110–121.

51. Bian, X., Yang, S., Chen, J., Ping, Y., Zhou, X., Wang, Q., Jiang, X., Gong, W., Xiao, H., Du, L., et al. (2007). Preferantial expression of chemokine receptor CXCR4 by highly malignant human gliomas and its association with poor patient survival. Neurosurgery *61*, 570–579.

52. Tang, C., and Guo, W. (2021). Implantation of a mini-osmotic pump plus stereotactical injection of retrovirus to study newborn neuron development in adult mouse hippocampus. STAR Protoc. *2*, 100374.

53. Alvarez-Breckenridge, C.A., Yu, J., Price, R., Wojton, J., Pradarelli, J., Mao, H., Wei, M., Wang, Y., He, S., Hardcastle, J., et al. (2012). NK cells impede glioblastoma virotherapy through NKp30 and NKp46 natural cytotoxicity receptors. Nat. Med. *18*, 1827–1834.

54. Van Den Bossche, W.B.L., Kleijn, A., Teunissen, C.E., Voerman, J.S.A., Teodosio, C., Noske, D.P., Van Dongen, J.J.M., Dirven, C.M.F., and Lamfers, M.L.M. (2018). Oncolytic virotherapy in glioblastoma patients induces a tumor macrophage phenotypic shift leading to an altered glioblastoma microenvironment. Neuro. Oncol. *20*, 1494–1504.

55. Isci, D., D'uonnolo, G., Wantz, M., Rogister, B., Lombard, A., Chevigné, A., Szpakowska, M., and Neirinckx, V. (2022). Patient-oriented perspective on

chemokine receptor expression and function in glioma. Cancers. *14, 130*.

56. Tischer, B.K., Kaufer, B.B., Sommer, M., Wussow, F., Arvin, A.M., and Osterrieder, N. (2007). A self-excisable infectious bacterial artificial chromosome clone of varicella-zoster virus allows analysis of the essential tegument protein encoded by ORF9. J. Virol. *81*, 13200–13208.

57. Todo, T., Martuza, R.L., Rabkin, S.D., and Johnson, P.A. (2001). Oncolytic herpes simplex virus vector with enhanced MHC class I presentation and tumor cell killing. Proc. Natl. Acad. Sci. U. S. A. *98*, 6396–6401.

58. Goins, W.F., Huang, S, Hall, B., Marzulli, M., Cohen, J.B., and Glorioso, J.C. (2020). Engineering HSV-1 Vectors for Gene Therapy. In: Herpes Simplex Virus: Methods and Protocols, Methods Mol. Biol. Springer Science, *2060, Chapter 4*.

59. Marconi, P., and Manservigi, R. (2014). Herpes simplex virus growth, preparation, and assay. Methods Mol. Biol. *1144*, 19–29.

60. Kroonen, J., Nassen, J., Boulanger, Y.G., Provenzano, F., Capraro, V., Bours, V., Martin, D., Deprez, M., Robe, P., and Rogister, B. (2011). Human glioblastoma-initiating cells invade specifically the subventricular zones and olfactory bulbs of mice after striatal injection. Int. J. Cancer *129*, 574–585.

829 Table 1: Primers used for RT-qPCR

	Forward	Reverse
HSV-1 gD	GCCCCGCTGGAACTACTATG	TTATCTTCACGAGCCGC-AGG
sTRAIL	CATCGAGAACGAGATCGCCC	TGTGTTGCTTCTTCCTCTGGT
SOX2	AGTCTCCAAGCGACGAAAAA	TTTCACGTTTGCAACTGTCC
POU3F2	CTGACGATCTCCACGCAGTA	GGCAGAAAGCTGTCCAAGTC
SALL2	ACTCCTCTGGGGTGACCTTT	GGAGTGGTAGTGGAGGTGGA
HSV-1 gD	GCCCCGCTGGAACTACTATG	TTATCTTCACGAGCCGC-AGG
sTRAIL	CATCGAGAACGAGATCGCCC	TGTGTTGCTTCTTCCTCTGGT
18S	AACTTTCGATGGTATCGCCG	CCTTGGATGTGGTAGCCGTTT
hTBP	ACAGCCTGCCACCTTACG	TGCCATAAGGCATCATTGGACTA

830

FIGURE LEGENDS

Figure 1:

Schematic representation of oHSV/Nb-gD and oHSV/Nb-gD:sTRAIL genomes.

Figure 2:

Efficacy of the oHSV de-targeting and re-targeting.

(A) De-targeting was evaluated by infection of J1.1-2, J/A (J1.1 HVEM$^+$) and J/C (J1.1 Nectin$^+$) cells were infected for 72 hours at different MOI with the recombinant oHSV expressing either WT gD (oHSV/gD) or gD modified by the insertion of an anti-hCXCR4 nanobody (oHSV/Nb-gD). Both viruses express eGFP under the control of pICP6, allowing the visualization of infected cells by epifluorescence microscopy. Scale bar represents 5 mm.

(B) Re-targeting was evaluated on U87MG and U87MG CXCR4$^+$ cells. Cells were plated in 96 well plates, infected with oHSV/gD or oHSV/Nb-gD (MOI 0.1) and Incubated in Incucyte® S3 for real-time analyses during 72hpi. GFP expression and cell confluency were quantified every 6 hours. Bars represent the Green area/phase area expressed as the mean ± SEM of four wells. Statistical significance was determined by ordinary two-way ANOVA with Bonferroni multiple comparisons of means with a single pooled variance. (ns: non-significant, **** p<0,0001). Images were taken every 6 hours and representative images taken at 72hpi are shown. Scale bars represent 2 mm. Additional representative whole-well images taken at 24, 48 and 72 hours are shown in Figure S2. See also growing curve of oHSV/gD and oHSV/Nb-gD in U87MG CXCR4$^+$ cells in Figure S3.

Figure 3

Efficacy of the oHSV retargeting in patient-derived GSCs.

(A) Patient-derived GSC cells (T08, T013, T018 and T033), U87MG or U87MG CXCR4^{+} cells were cultured as tumorospheres and further dissociated for flow cytometry quantification of the percentage of cells expressing CXCR4 (APC^{+}) at the cell membrane. Bars represent the means ± SEM of four independent experiments. Statistical significance was determined by Kruskal-Wallis (Primary cells, **p < 0.001) or Mann-Whitney (U87MG cells, *p < 0.05) test. **(B)** Overlayed histograms of a representative analysis allowing the comparison between endogenous and ectopic CXCR4 expression**.**

Stemness features (expression of SOX2, POUF3 and SALL2) analyzed by RT-qPCR are depicted in Figure S4.

(C) Tumorospheres cultured in 24-well plates were infected with oHSV/gD or oHSV/Nb-gD (10^{6}PFU/ml). Forty-eight hours post infection, cells were dissociated and the eGFP fluorescence was analyzed by flow cytometry. Bars represent the means ± SEM of three independent experiments. Statistical significance was determined by ordinary 2-way ANOVA with Bonferroni's multiple comparisons of means (**p < 0.001). Raw data (overlaid histograms) representative of one experiment are shown in Figure S5.

(D) Tumorospheres cultures in 24-well plates and infected for 48h by oHSV/Nb-gD (10^{6} PFU/ml) were either analyzed by epifluorescence for eGFP detection (left panels) or fixed for immunostaining of nestin (white) or CXCR4 (Red) and GFP detection (green). Nuclei were labeled with DAPI (Blue). Images were recorded with a NIKON A1R confocal microscope. Scale bars represent 100 µm.

See also Figure S6 for real-time eGFP quantification and images of T033 tumorospheres infected with oHSV/gD or oHSV/Nb-gD at a higher titer (10^{7} PFU/ml)

Figure 4

Efficacy of the oHSV arming.

(A) The replication efficacy of the non-armed (oHSV/Nb-gD) and sTRAIL-armed (oHSV/Nb-gD:sTRAIL) oncolytic viruses was evaluated with a growing curve assay. U87MG CXCR4$^+$ cells were infected at a MOI of 1 and supernatant was harvested at 24, 48 and 72 hours post infection and used for titration as previously described [59]. The number of foci was calculated based on Incucyte®S3 imaging. Bars represent mean ± SEM (PFU/ml) of three independent experiments. The lack of statistical difference is confirmed by unpaired *t*-test analysis**.**

(B) PARP and caspase 3 cleavage was evaluated by Western blot analysis on total cell extracts from U87MG CXCR4$^+$ cells infected for 18h by oHSV/Nb-gD or oHSV/Nb-gD:sTRAIL (MOI: 0.5 or 1). gD and alpha-tubulin detection were used as infection or loading control, respectively.

(C) Apoptosis was measured at different time points by flow cytometry using annexin V/DAPI labeling of U87MG CXCR4$^+$ cells infected by oHSV/Nb-gD or oHSV/Nb-gD:sTRAIL (MOI: 5-. The percentage of apoptotic cells corresponds to early (Annexin V$^+$/DAPI$^-$) and late apoptotic (Annexin V$^+$/DAPI$^+$) cells. Percentages of apoptotic cells upon infection at other MOI (1, 5 and 10) er shown in Figure S7. In parallel, cells were incubated with resazurin to evaluate the viability upon oHSV infection. Bars and dots represent the means ± SEM of three independent experiments. Statistical significance was determined by ordinary 2-way ANOVA with Bonferroni's multiple comparisons of means (***$p < 0.001$).

(D and E) Patient-derived GSCs (T08, T013, T018 and T033) were cultured as tumorospheres in 24-well plates and infected with oHSV/Nb-gD or oHSV/Nb-gD:sTRAIL (10^6PFU/ml). gD and sTRAIL relative expression was analyzed 48hpi by RT-qPCR as

illustrated by a representative experiment. gD **(D)** and sTRAIL **(E)** mRNA level in oHSV/Nb-gD:sTRAIL-infected T08 is considered as the base line**.** (ND: not detected).

Figure 5

In vivo **efficacy of oHSV/Nb-gD and oHSV/Nb-gD:sTRAIL.**

(A) Schematic representation of the experimental settings. Nude mice were engrafted with U87MG CXCR4^{+}Luc^{+} cells and virus or PBS was injected in the tumor on day 7. Mice were sacrificed on day 22 (n= 9 in each group). **(B)** Mice were regularly weighed, and for each mouse, the weight change is expressed as a percentage to the weight on day 0, considered as equal to 100%. **(C)** Bioluminescence activity was recorded with Xenogen IVIS 50® on day 6, 13 and 20 after engraftment. See also Figure S9 for Bioluminescence imaging**. (B)** and **(C)** represent the means ± SEM (n=9 in each group). Statistical significance was determined by 2-way ANOVA with Tukey's multiple comparisons of means. (* p<0.05; **p<0.01; *** p<0.001).

(D to F) On day 22, brain from five mice were sectioned for immunostaining of human vimentin and the measurement of the tumor volume by 3D reconstruction **(D)**. Representative pictures of serial sections of 2 mice/group as well as the estimated volume of the corresponding tumor are shown in **(E)** Scale bars represent 1 mm. Data represent the means ± SEM. Statistical significance was determined by Krustall-Wallis test (*p < 0.05). In parallel, brain from the 4 other mice were divided into 3 parts (frontal, middle and occipital) which were frozen and treated independently for RNA extraction and RT-qPCR analysis of hCXCR4 expression **(F)**. For each sample, PBS-treated mice (middle sample) is considered as the base line. Bars represent the means ± SEM. Statistical significance was determined by two-way ANOVA with Tukey's multiple comparisons of means with a single pooled variance (*p < 0.05, **p < 0.01).

Figure 6.

Survival assay upon oHSV/Nb-gD or oHSV/Nb-gD:sTRAIL treatment.

(A) Schematic representation of the survival assay experimental settings. **(B)** Bioluminescence activity of nude mice engrafted with 5 x 10^4 U87MG CXCR4 Luc^+ cells were recorded with Xenogen IVIS 50®on day 5 (two days before treatment) and 13 (6 days after treatment). Bars represent the means ± SEM. Statistical significance was determined by two-way ANOVA with Tukey's multiple comparisons of means. (**p<0.01). See also Figure S10B for Bioluminescence imaging **(C)** Probability of survival of mice treated with PBS (n=7), oHSV/Nb-gD (n=6) or oHSV/Nb-gD:sTRAIL (n=5). The red arrow indicates the day of treatment (Day 7). Statistical significance was determined by log-ranked (Mantel-Cox) test (**** p<0.0001). See also Figure S10A for weight follow-up.

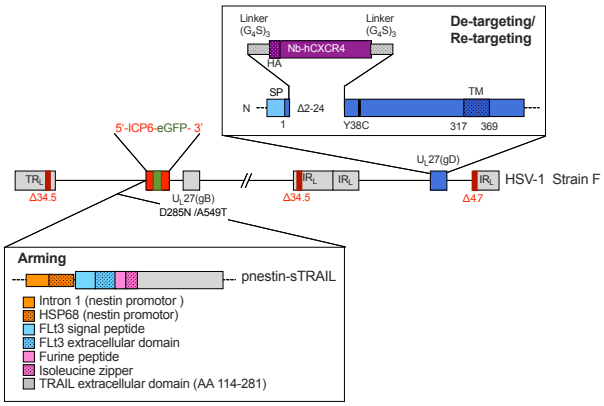

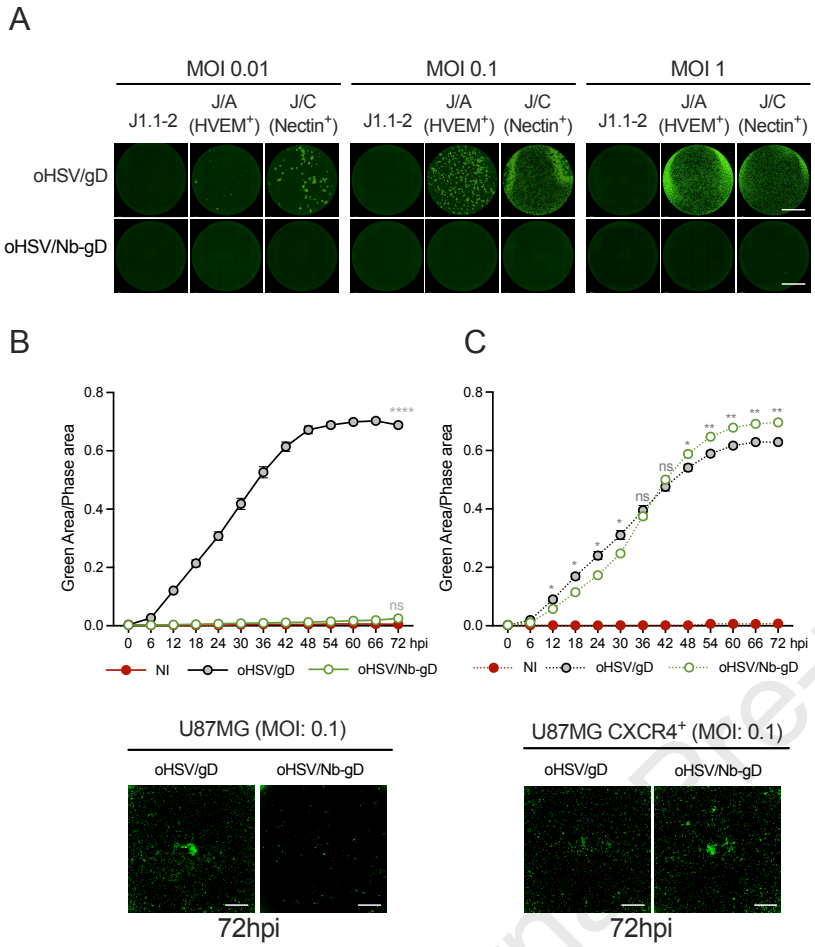

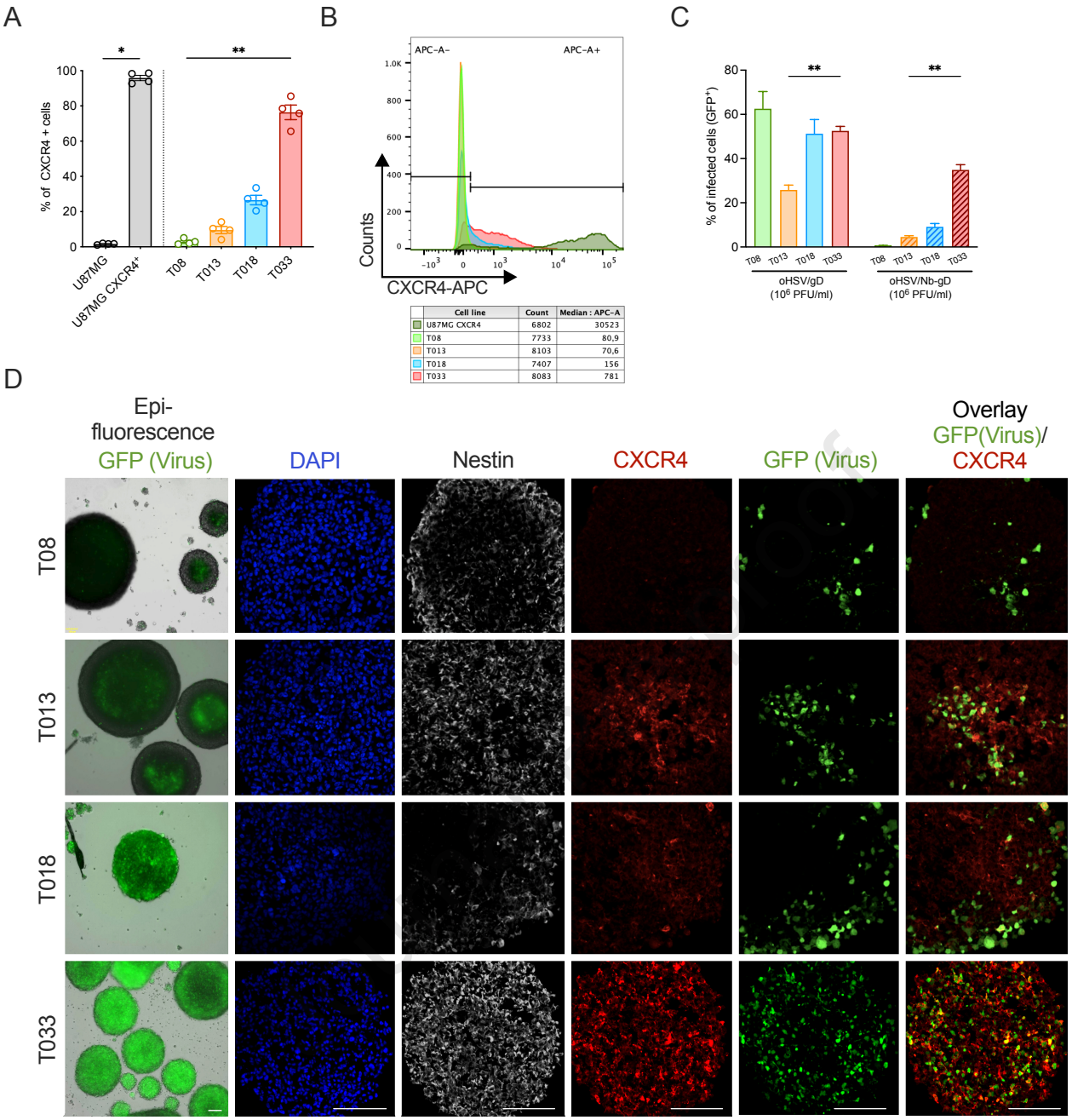
A
% of CXCR4 + cells
U87MG
U87MG CXCR4+
T08
T013
T018
T033
B
APC-A-
APC-A+
Counts
CXCR4-APC
Cell line | Count | Median : APC-A
U87MG CXCR4 | 6802 | 30523
T08 | 7733 | 80,9
T013 | 8103 | 70,6
T018 | 7407 | 156
T033 | 8083 | 781
C
% of infected cells (GFP+)
oHSV/gD (10^6 PFU/ml)
oHSV/Nb-gD (10^6 PFU/ml)
D
Epi-fluorescence GFP (Virus)
DAPI
Nestin
CXCR4
GFP (Virus)
Overlay GFP(Virus)/ CXCR4
T08
T013
T018
T033

A

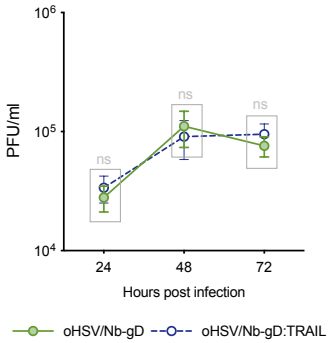

B

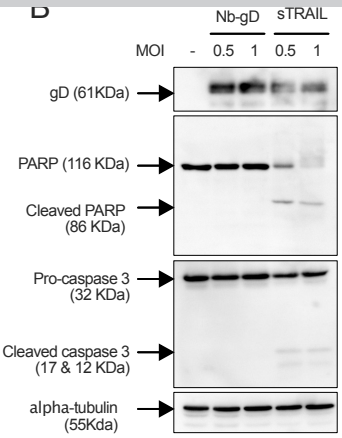

C

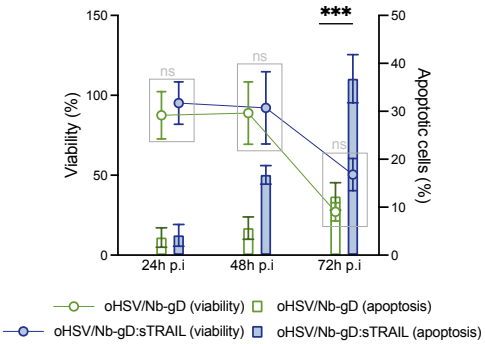

D

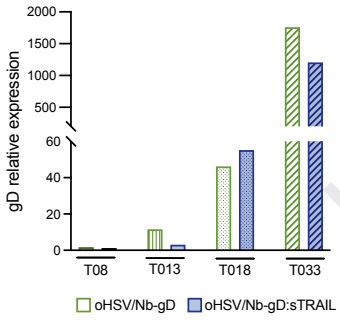

E

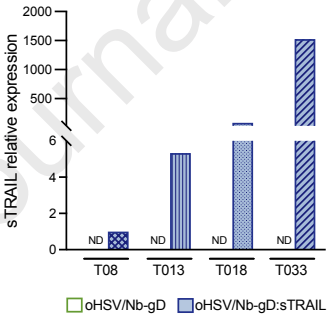

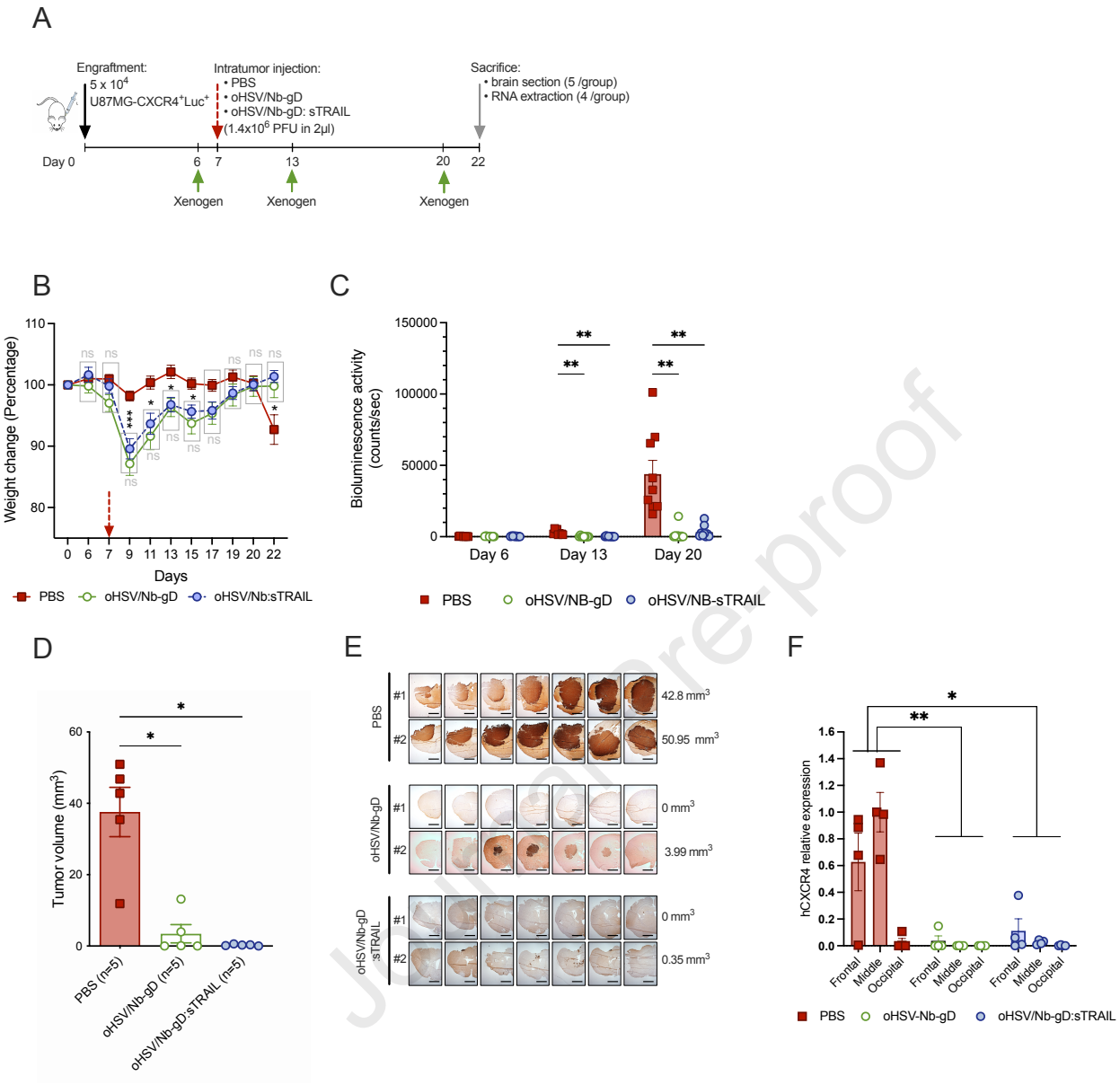
A
Engraftment:
5 x 10^4
U87MG-CXCR4+Luc+
Intratumor injection:
• PBS
• oHSV/Nb-gD
• oHSV/Nb-gD: sTRAIL
(1.4x10^6 PFU in 2µl)
Sacrifice:
• brain section (5 /group)
• RNA extraction (4 /group)
Day 0
6
7
13
20
22
Xenogen
Xenogen
Xenogen
B
Weight change (Percentage)
Days
PBS
oHSV/Nb-gD
oHSV/Nb:sTRAIL
C
Bioluminescence activity (counts/sec)
Day 6
Day 13
Day 20
PBS
oHSV/NB-gD
oHSV/NB-sTRAIL
D
Tumor volume (mm3)
PBS (n=5)
oHSV/Nb-gD (n=5)
oHSV/Nb-gD:sTRAIL (n=5)
E
PBS
oHSV/Nb-gD
oHSV/Nb-gD :sTRAIL
42.8 mm3
50.95 mm3
0 mm3
3.99 mm3
0 mm3
0.35 mm3
F
hCXCR4 relative expression
Frontal
Middle
Occipital
PBS
oHSV-Nb-gD
oHSV/Nb-gD:sTRAIL

A

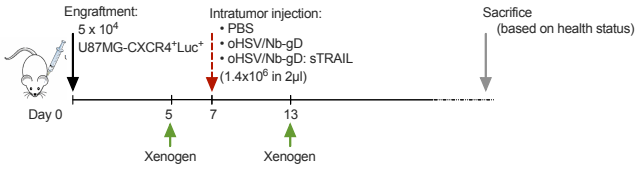

B

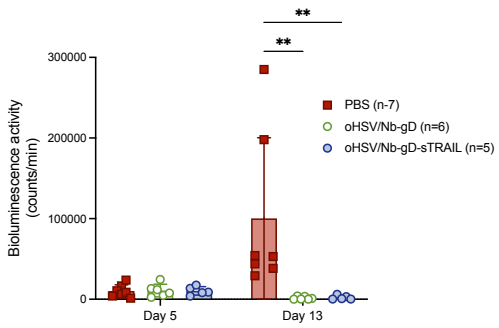

C

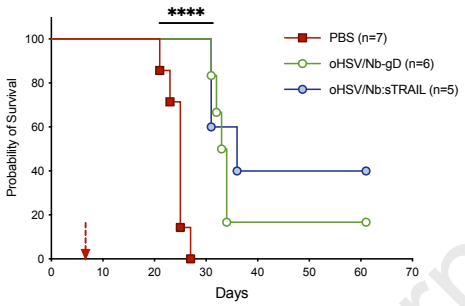

eTOC SYNOPSIS

Sanchez-Gil and colleagues show as a proof-of-principle that nanobodies can be used to retarget an oncolytic herpesvirus to a sub-population of GBM cells. An anti-CXCR4 nanobody-retargeted virus can infect U87MG and patient-derived GBM stem-like cells on a CXCR4-dependent manner and trigger apoptosis when armed with sTRAIL. In an orthotopic xenograft mouse model, this virus decreases tumor growth and increases survival.